Journal of Nuclear Materials 385 (2009) 339–345

Contents lists available at ScienceDirect

Journal of Nuclear Materials

journal homepage: www.elsevier.com/locate/jnucmat

Influence of oxide layer morphology on hydrogen concentration in tin and niobium containing zirconium alloys after high temperature steam oxidation

Mirco Große [a,*], Eberhard Lehmann [b], Martin Steinbrück [a], Guido Kühne [b], Juri Stuckert [c]

[a] Institute for Materials Research I, Forschungszentrum Karlsruhe, Germany
[b] Paul Scherrer Institute Villigen, Spallation Neutron Source Division, Switzerland
[c] Institute for Materials Research III, Forschungszentrum Karlsruhe, Germany

ARTICLE INFO

PACS:
28.20.Fc
28.41.Bm
66.30.−h
32.80.−t
81.65.Mq

ABSTRACT

The influence of the oxide layer morphology on the hydrogen uptake during steam oxidation of (Zr,Sn) and Zr–Nb nuclear fuel rod cladding alloys was investigated in isothermal separate-effect tests and large-scale fuel rod bundle simulation experiments. From both it can be concluded that the concentration of hydrogen in the remaining metal strongly depends on the existence of tangential cracks in the oxide layers formed by the tetragonal – monoclinic phase transition in the oxide, known as breakaway effect. In these cracks hydrogen is strongly enriched. It results in very local high hydrogen partial pressure at the oxide/metal interface and in an increase of the hydrogen concentration in the metal at local regions where such cracks in the oxide layer exist. Due to this effect the hydrogen uptake of the remaining zirconium alloy does not depend monotonically on temperature. Differences between (Zr,Sn) and Zr–Nb alloys are caused by differences in the hydrogen production due to different oxidation kinetics and in the crack forming phase transformation in the oxides as well as in the mechanical stability of the oxides.

1. Introduction

In the framework of loss of coolant accident (LOCA) and severe fuel damage (SFD) nuclear accident research the behavior of hydrogen produced by steam oxidation of fuel rod cladding tubes was studied in a lot of experiments [1–3]. The coexistence of hot fuel and cooling water results in a strongly exothermic reaction between cladding and steam with the consequence of production of protons:

$$\mathrm{Zr(m)} + 2\mathrm{H_2O(g)} + 4\mathrm{e(ox/g)} \Longleftrightarrow \mathrm{ZrO_2(ox)} + (2-x)\mathrm{H_2(g)} + 2x\mathrm{H_{ab}(m)} + 4\mathrm{e(m/ox)}$$

Zr(m) represents regular zirconium atoms in the metallic phase lattice, e(ox/g) is the electron produced by oxygen vacancy formation at the oxide/gas interface and e(m/ox) the electron consumed by a proton at the metal/oxide interface. The produced protons can be released as $H_2(g)$ into the environment or absorbed by the metal $H_{ab}(m)$. In this last case, protons have to diffuse through the growing oxide layer as suggested by [4]. Absorption influences the hydrogen source term, at least temporally. It results in an embrittlement of the cladding with the consequence of increasing risk of breaking the cladding connected with a loss of barrier effect and strong heat production by the oxidation of the inner cladding surface.

The hydrogen uptake of the remaining zirconium alloy during isothermal steam oxidation was studied experimentally in [5–9]. As [7,8] have shown hydrogen concentration in the remaining zirconium alloy is strongly influenced by the stability of the oxide layer formed during steam oxidation. At certain temperatures depending on the alloy composition the oxide growth starts with an undercooled tetragonal structure. When a certain oxide layer thickness is reached the oxide structure transforms to monoclinic. This martensitic transformation is connected with a volume change and the formation of micro and macro cracks in radial and hoop direction. The phenomenon is known as breakaway effect. In [7] it was reported that the hydrogen concentration is as higher as earlier the breakaway starts. In [8] the hydrogen uptake of the classical cladding material Zry-4 and the E110 used in Russian type VVER reactors is compared. Whereas hydrogen is detected in Zry-4 only at 1273 K up to 30 at.% hydrogen was found in E110 at all temperatures investigated between 1173 and 1473 K.

Theoretical models to describe this process have been developed in [9,10]. Basis of both models are compact oxide layers and parabolic oxidation kinetic. These models divide the hydrogen uptake into two phases. In the initial phase of steam oxidation, the hydrogen chemical activity in the gas phase is higher than in the residual metal. From a diffusion model it is concluded that the hydrogen concentration in the metal $c_H(m)$ increases with

* Corresponding author. Fax: +49 7247 82 4567.
E-mail address: Mirco.Grosse@IMF.FZK.de (M. Große).

0022-3115/$ - see front matter © 2008 Elsevier B.V. All rights reserved.
doi:10.1016/j.jnucmat.2008.12.021

oxidation time t by the power of +3/8 [10]. After a certain time a dynamic equilibrium is established between the hydrogen chemical activities in metallic zirconium, zirconium oxide and the surrounding gas atmosphere.

The equilibrium between hydrogen concentration in the metal phase $c_H(m)$ and partial pressure in the gas atmosphere p_{H_2} can be described by the well known Sieverts' law [11]:

$$c_H(m) = K_S \cdot p_{H_2}^{\frac{1}{2}} \quad (1)$$

$$K_S = \exp\left(\frac{\Delta S}{R} - \frac{\Delta H}{RT}\right) \quad (2)$$

$c_H(m)$ is the concentration of absorbed hydrogen in the metal phases in at.%, p_{H_2} the hydrogen partial pressure in Pa, Ks the Sieverts' constant in $Pa^{-1/2}$, S the entropy, H the enthalpy, T the absolute temperature and R the universal gas constant (8.31 J mol^{-1} K^{-1}).

Due to the decrease of the oxidation rate with time resulting from the parabolic reaction kinetics the hydrogen partial pressure in the gas decreases and with it the concentration in the metal. In [10] a decrease of the hydrogen concentration in the metal with time by the power of $-1/8$ is predicted by theoretical modeling of this process, whereas in [9] $c_H(m) \sim t^{-\frac{1}{4}}$ was determined experimentally. The temperature dependence of the hydrogen concentration is, at least between 1373 and 1573 K, of the Arrhenius type. The differences between [9] and [10] are caused by thermo-hydraulic conditions. A laminar gas flow is assumed in [10], whereas in [9] turbulent gas flow was realized experimentally. Strong differences from an Arrhenius like temperature dependence were found for the Zr–Nb alloy E110 used in a large scale bundle simulation test in [12].

In this work the reasons for these differences from the expected hydrogen uptake behavior are studied in isothermal steam oxidation experiments and on materials taken from large scale bundle simulation tests.

2. Experimental details

2.1. Materials

The investigations comprise commercial charges of the classical cladding alloys Zircaloy-4 (Zry-4) and E110 (used in Russian VVER reactors, produced by JSC ChMP) and of the advanced materials M5 and DUPLEX (used in Western European PWRs, produced by FRAMATOME/AREVA). Zry-4, M5 and E110 are homogeneous materials. The DUPLEX material consists of a Zry-4 bulk and a tin depleted D4 layer with a thickness of 150 μm at the outer surface, reducing the oxidation susceptibility. The chemical compositions of the investigated materials are given in Tables 1a and 1b in wt% and at.%, respectively.

2.2. Isothermal steam oxidation experiments

Segments from original cladding tubes with outer and inner diameters of 10.75 mm (E110: 9.15 mm) and 9.25 mm (E110: 7.50 mm), respectively, and a length of 20 mm were used for the investigations. The specimens were annealed isothermally in a resistance heated tube furnace in flowing argon/steam atmosphere. The flow rates for argon and steam were 50 l h^{-1} and 50 g h^{-1}, respectively. Annealing temperatures and times were varied. Due to the open tube segments, oxidation occurs at both, the outer and inner surface. One consequence is that for the DUPLEX material the hydrogen uptake is composed by the absorption through the D4 layer at the outer surface and of the Zry-4 at the inner surface. More details about the annealing are given in [9]. The oxidation kinetics determined for various temperatures are published in [13].

Table 1a
Chemical composition of the investigated alloys in wt%.

Alloy	O	Cr	Fe	Zr	Nb	Sn
Zry-4	0.14	0.10	0.21	~98.0	–	1.50
D4	0.14	0.20	0.50	~98.6	–	0.50
E110	0.05	–	<0.01	~98.9	0.97	–
M5	0.14	0.003	0.034	~98.8	1.00	–

Table 1b
Chemical composition of the investigated alloys in at.%.

Alloy	O	Cr	Fe	Zr	Nb	Sn
Zry-4	0.80	0.18	0.34	~97.5	–	1.15
D4	0.80	0.35	0.82	~97.7	–	0.38
E110	0.29	–	<0.02	~98.7	0.95	–
M5	0.80	0.005	0.056	~98.1	0.98	–

2.3. Large scale bundle simulator quench tests

E110 and Zry-4 were used as cladding material for fuel rod simulators bundles (length 2.5 m) applied in the large severe accident tests QUENCH-12 [14] and QUENCH-13 [15], respectively. The temperature scenarios of the tests are given in Figs. 1 and 2, respectively. In order to get information about the oxidation of the zirconium alloy after certain test phases, up to three corner rods can be withdrawn during the test. These corner rods are also used for studying the hydrogen uptake.

During the QUENCH-12 test corner rods (material E110) were withdrawn after the pre-oxidation phase (rod D), in the transient phase before water quenching at about 1823 K (rod F), and 20 h after the test (rod B). In the QUENCH-13 test a corner rod (material: Zry-4) was withdrawn after failure of the AgInCd control rod simulator in the bundle center at about 1550 K (rod B) and two corner rods were taken one day after the test (rods C and D).

Due to the different temperature scenarios the tests are not comparable. However, a strong axial temperature gradient provides the possibility to study the temperature dependence of the hydrogen uptake and the influence of oxide morphology on the temperature history.

2.4. Determination of hydrogen concentration by means of neutron radiography

The total microscopic neutron cross section of hydrogen $\sigma_{tot}(H)$ is much higher than the cross section of zirconium $\sigma_{tot}(Zr)$ This provides the possibility to determine the hydrogen concentration in zirconium and zirconium alloys by quantitative analysis of neutron radiographs. The macroscopic total neutron cross section Σ_{tot} of a sample is given by:

$$\Sigma_{tot} = \sum_i N_i \sigma_{tot}(i) = \frac{-\ln\left(\frac{I-I_B}{I_0-I_B}\right)}{s} \quad (3)$$

N is the atomic number density and $\sigma_{tot}(i)$ the microscopic cross section of the isotope i, I_0, I and I_B are the primary, the transmitted and the background intensity of the neutron beam, respectively and s is the path length of the beam through the material. From Eq. (3) a linear correlation between total macroscopic neutron cross section of the sample and N_H/N_{Zr} atomic ratio results:

$$\frac{N_H}{N_{Zr}} = \frac{\Sigma_{total} - N_{Zr}\sigma_{Zr}}{N_{Zr}\sigma_H} \quad (4)$$

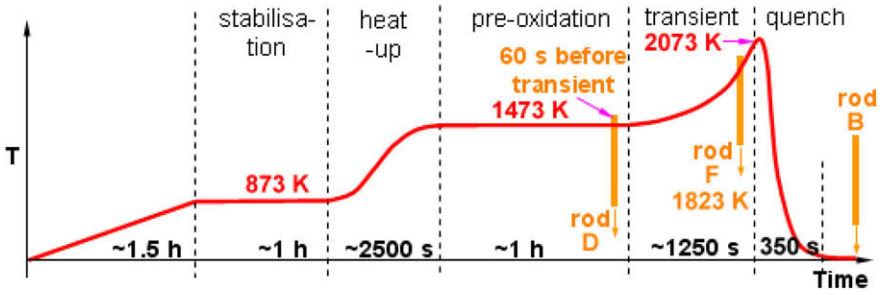

Fig. 1. Temperature scenario of the QUENCH-12 large scale bundle test (material E110).

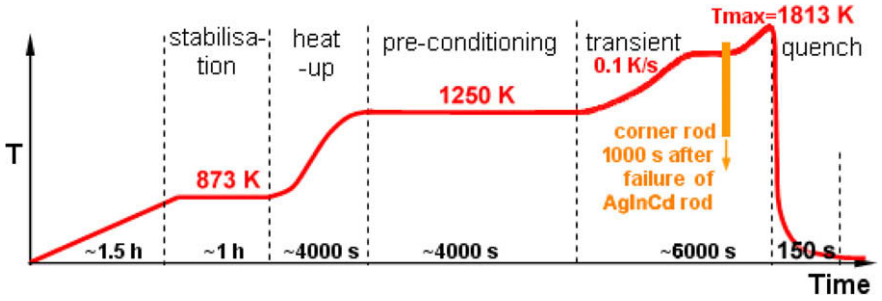

Fig. 2. Temperature scenario of the QUENCH-13 large scale bundle test (material Zry-4).

σ_{Zr} and σ_H depend on the experimental setup (neutron spectrum, energy dependence of detector efficiency). Therefore, the correlation parameters were determined by Zry-4 calibration specimens with known hydrogen concentration. A detailed description of the method and the calibration of the dependence of the total macroscopic neutron cross section on the N_H/N_{Zr} atomic ratio are given in [16]. Measurements with hydrogen free DUPLEX and E110 specimens and E110 specimens with known hydrogen content have shown that the calibration can be applied also for these materials. Due to the chemical composition of M5 is very similar to E110 the correlation found in [16] was also used for the hydrogen determination in M5.

The neutron radiography experiments were performed at the ICON facility at the SINQ neutron source at PSI (Villigen, Switzerland) [17]. The radiography image was taken by a Peltier-cooled CCD camera (type DV436 from Andor Technology, Northern Ireland), combined with Gd converter/scintillator screen of 10 μm thickness. The images with a size of 28×28 mm comprise 2048×2048 pixels. The pixel to pixel distance is 13 μm. The hydrogen concentration in the remaining metal of the cladding tube segments oxidized isothermally and of corner rods of large scale QUENCH tests was determined using Eq. (4).

3. Results and discussion

3.1. Isothermal oxidation

As an example, the neutron radiographs of the investigated materials oxidized in steam at 1273 K for 1 h are given in Fig. 3. The darker the specimen appears in the radiography image, the lower the neutron transmission and with it according to the Eqs. (3) and (4) the higher the hydrogen concentration. The gradients in the transmitted intensity beyond the specimens are caused only by the different pass lengths of the neutron beams at different radial positions due to the tube shape. Hydrogen is homogenously distributed in the specimens. Differences in the neutron transmission between the specimens are obvious. From the neutron transmissions the hydrogen concentrations in the remaining metal were determined using Eq. (4). The results are given in Table 2.

Strong differences in the hydrogen concentrations were found between the materials for one temperature but also between the oxidation temperatures for one material.

At 1273 K the both (Zr,Sn) alloys Zry-4 and DUPLEX show the highest hydrogen concentration, whereas at 1373 K the hydrogen uptake is the highest in the Zr–Nb alloys. Its concentration increases between 1273 and 1373 K in the Zr–Nb alloys but decreases in the (Zr,Sn) alloys. Zry-4 has the highest concentration values of the (Zr,Sn) alloys at both temperatures. A comparison between the two Zr–Nb alloys shows that the hydrogen concentration is in M5 higher than in E110 after steam oxidation at both temperatures.

According to Eq. (1), the reasons for these findings are different hydrogen partial pressures at the sample surfaces due to different oxidation kinetics and/or due to different morphologies of the oxide layers.

Fig. 4 gives the light optical micrographs of the samples cross section of the investigated materials, oxidized at 1273 K. From the Zr–O phase diagram and the oxidation kinetics it can be concluded that Zr–Nb alloys form oxides with monoclinic structure whereas in the (Zr, Sn) alloys the oxide starts to grow with tetragonal structure and transforms to monoclinic structure after reaching a certain thickness [18]. This martensitic phase transformation is connected with a change in volume, with residual mechanical stresses and formation of micro- and macro-cracks in the oxide layer, which can be seen in the micrographs of DUPLEX (at the inner surface) and of Zry-4 (at the inner and the outer surface). The formed open cracks act as a 'hydrogen pumps': steam penetrates into the cracks and reaches the oxide/metal interface. Oxidation occurs at the interface and hydrogen remains in the cracks. Due to the high hydrogen partial pressure formed in the cracks a part of the hydrogen is absorbed by the metal. The total gas pressure decreases with the consequence that new steam flows into the cracks. The lower hydrogen concentration in the Zr–Nb alloys is

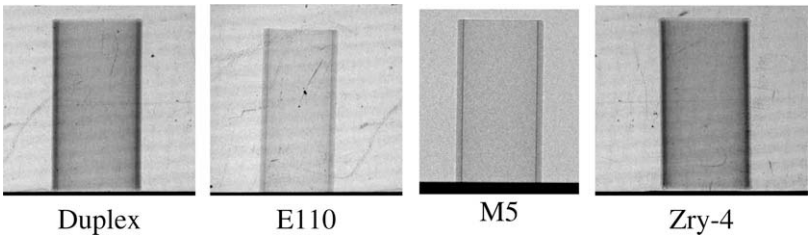

Fig. 3. Neutron radiographs of the investigated materials after 1 h steam oxidation at 1273 K.

caused by the lower oxidation rate and with it the lower hydrogen production during the steam oxidation. It is in contradiction to the findings in [8]. Maybe the lower impurity concentration in common E110 used in these investigations can explain the differences to [8] (see Fig. 5).

At 1373 K all investigated materials form compact tetragonal oxides without open macro-cracks. In spite of a smaller oxide layer thickness of the Zr–Nb specimens and with it a lower oxidation rate and hydrogen production the hydrogen concentrations are higher in these alloys than in the (Zr,Sn) alloys. It can be explained by larger β-Zr phase content in these materials which can absorb a higher amount of hydrogen than α-Zr. This is in agreement with the results given in [8]. The smaller hydrogen concentration of DUPLEX compared to Zry-4 shows the protective behavior of the D4 layer. The oxide layer at the outer surface does not show the breakaway effect at 1273 K. Also the so called 'tin lines', tin segregations in the oxide layers are not formed in DUPLEX. These tin segregations, which are typical for Zry-4, increase the numbers of grain boundaries and with it, they enhance diffusion. The reasons of the differences between the two Zr–Nb alloys E110 and M5 can not be clearly separated, because the differences in the diameters results in differences of the active surfaces of the specimens. However, the factor two in the hydrogen concentration between M5 and E110 can not be explained only by geometry effects. The oxide layers at E110 specimens seem to have a smaller content of radial micro-cracks. Maybe, the lower effective crack length across the oxide is an additional reason for the smaller hydrogen uptake.

Table 2
Hydrogen concentrations in the investigated alloys after 1 h steam oxidation at 1273 and 1373 K.

Alloy	c_H (at.%) at T = 1273 K	c_H (at.%) at T = 1373 K
DUPLEX	5.60	1.56
E110	1.89	2.94
M5	4.05	6.63
Zry-4	9.23	1.76

3.2. Fuel rod simulator bundle tests

In order to study the influence of oxide layer structure and morphology on the hydrogen uptake, the axial hydrogen distributions

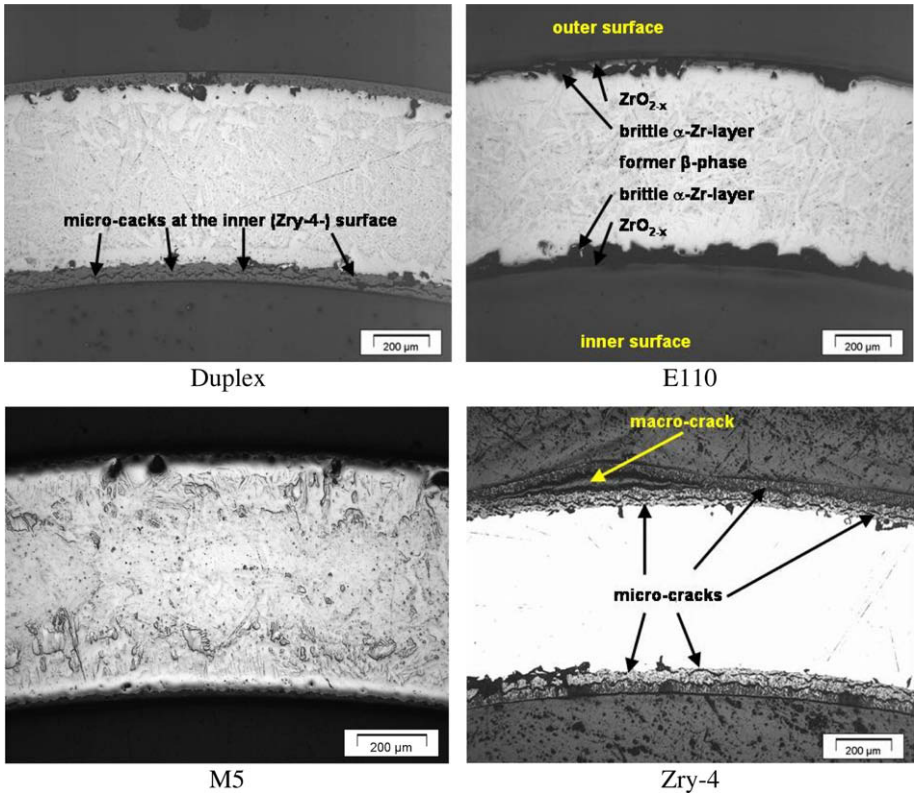

Fig. 4. Optical micrographs of sample cross sections after 1 h steam oxidation at 1273 K.

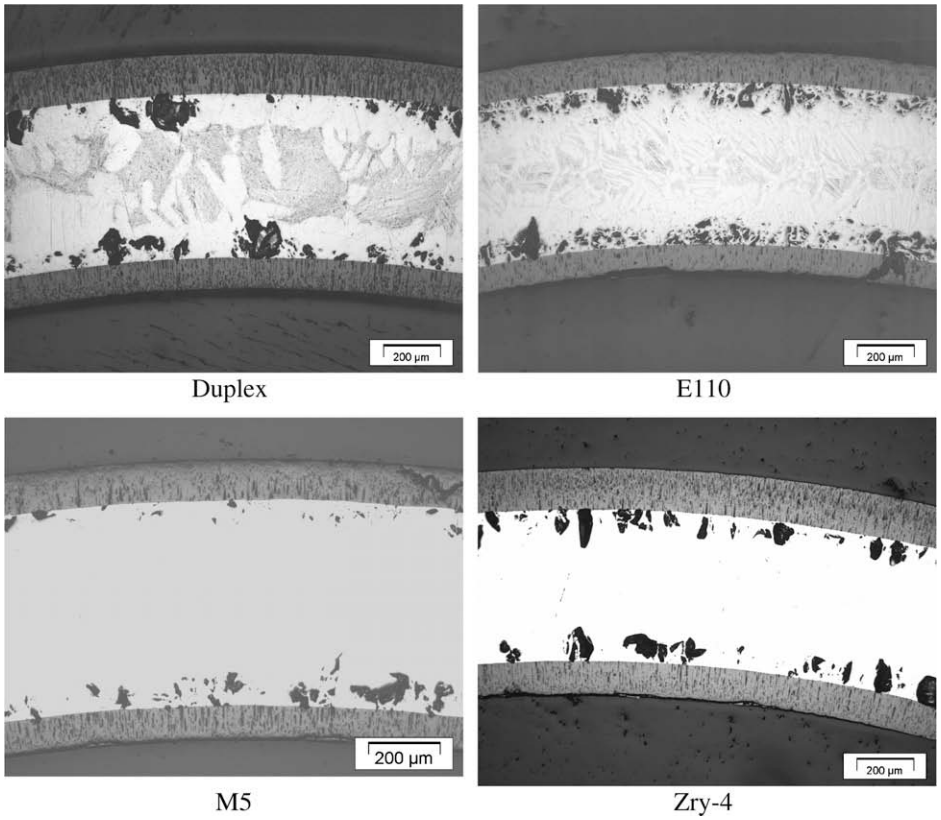

Fig. 5. Optical micrographs of sample cross sections after 1 h steam oxidation at 1373 K.

in the withdrawn corner rods can be used. These distributions are given for the corner rods withdrawn in the QUENCH-12 and -13 large scale tests in Figs. 6 and 7, respectively.

In all three corner rods of the QUENCH-12 bundle, distributions with two local maxima at $z \approx 850$ and 1080 mm were found. The local minima at $z \approx 970$ mm are at the position of the highest temperature.

Due to the long pre-oxidation time (see Fig. 1) a quasi-equilibrium state can be assumed for rod D. On this basis Eq. (2) can be applied.

In Fig. 8 the axial distributions of the pre-oxidation temperature ($T_{\text{fit,}}$ fitted from several thermo couples signals), the hydrogen concentration (c_{H} measured) and the hydrogen partial pressure (p_{H_2}) are given. Additionally, typical micrographs are included. A local maximum in the partial pressure could not be expected by the experimental conditions. Due to the flow from bottom to top the hydrogen partial pressure in the gas should increase monotonically with increasing axial height z. The maximal concentrations of about 35 at.% are unexpectedly high. The corresponding hydrogen partial pressure is about two orders of magnitude higher than the value measured in the off-gas by mass spectrometer at the end of the pre-oxidation phase.

These contradictions show that the hydrogen partial pressure in the gas bulk does not determine the hydrogen uptake of the remaining zirconium alloy but the very local partial pressure at the oxide-metal boundary. At the axial position of the highest corresponding hydrogen partial pressure, the oxide consists of a lot of small layers separated by open tangential cracks (see Fig. 8). It confirms the results of the isothermal oxidation tests. Also in these cracks hydrogen is enriched during steam oxidation and the 'hydrogen pump effect' occurs. At the position of the highest temperature compact oxides are formed. Due to the absence of large

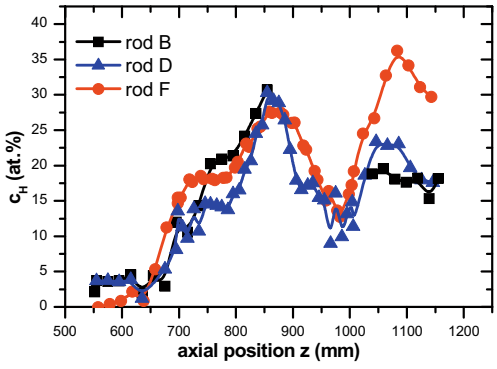

Fig. 6. Axial hydrogen distribution in the corner rods of the QUENCH-12 test.

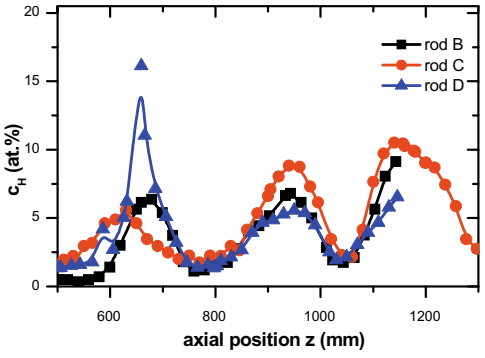

Fig. 7. Axial hydrogen distribution in the corner rods of the QUENCH-13 test.

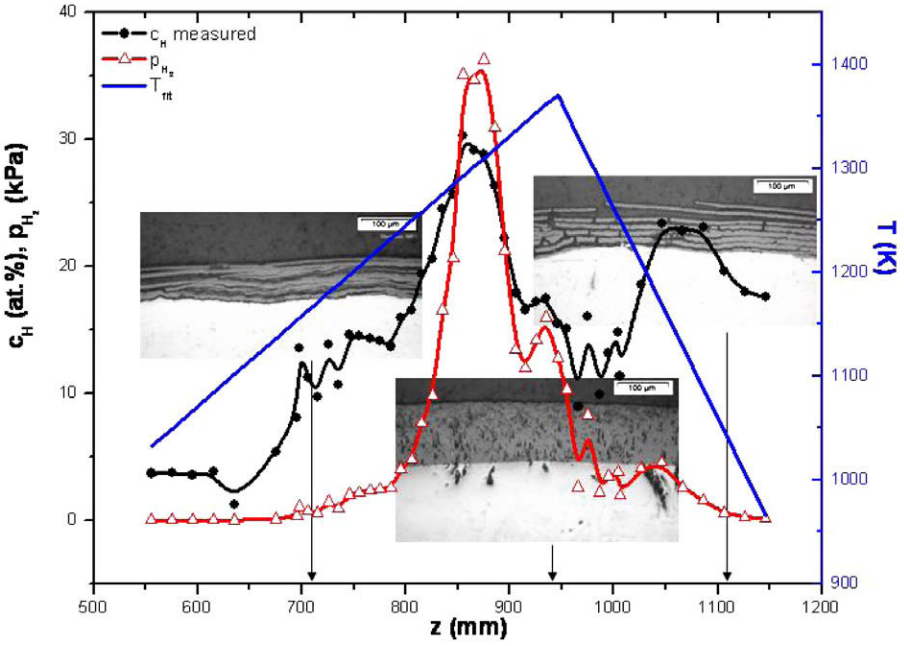

Fig. 8. Axial distribution of temperature, hydrogen concentration, partial pressure and optical micrographs of the microstructure in corner rod D of the QUENCH-12 bundle withdrawn after the pre-oxidation phase.

cracks the local hydrogen partial pressure at the surface and with it the hydrogen uptake is relative low.

The hydrogen distributions in the QUENCH-13 corner rods, given in Fig. 7, show three maxima at $z \approx 660$, 940 and 1150 mm and minima at $z \approx 760$ and 1040 mm. Also here are the reasons for the local maxima the crack formation in the oxide layer as shown in the micrographs included in Fig. 9.

Maximum hydrogen concentrations were found at axial position with tangential macro-cracks in the oxide layer.

The hydrogen concentrations are lowest at positions with compact oxides. The differences between the peaks of the hydrogen concentration at about $z \approx 660$ mm of the rods C and D, both withdrawn after the test, are remarkable. As Fig. 10 shows the crack density and size is significantly smaller in rod C than in rod D. A much higher maximum in the hydrogen concentration in rod D results at this position. The reason for the differences in the crack structure can be circumferential temperature fluctuation in the large scale fuel rod simulator bundle.

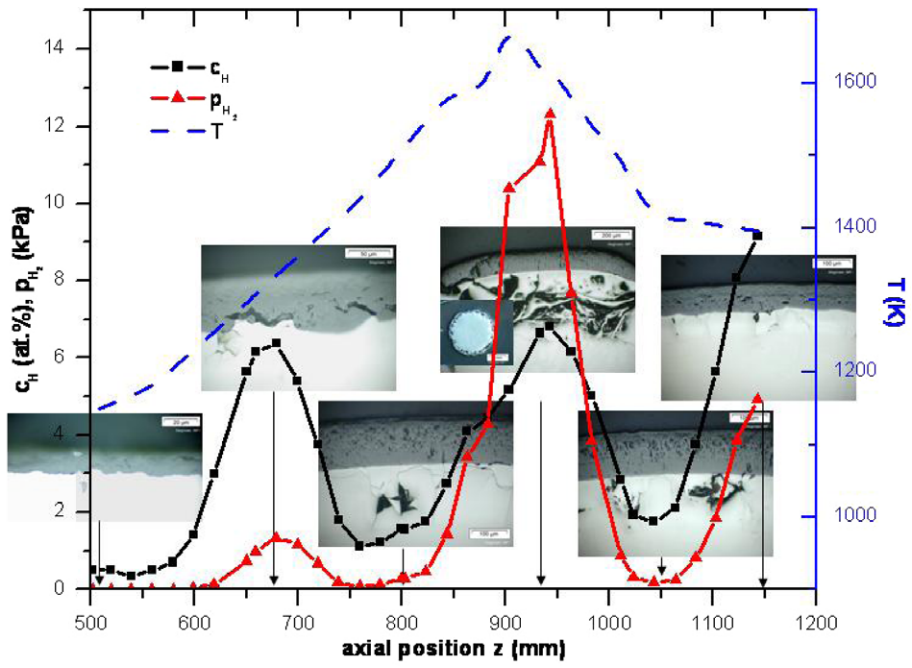

Fig. 9. Axial distribution of temperature, hydrogen concentration, partial pressure and optical micrographs of the microstructure in corner rod D of the QUENCH-13 bundle withdrawn after the pre-conditioning phase.

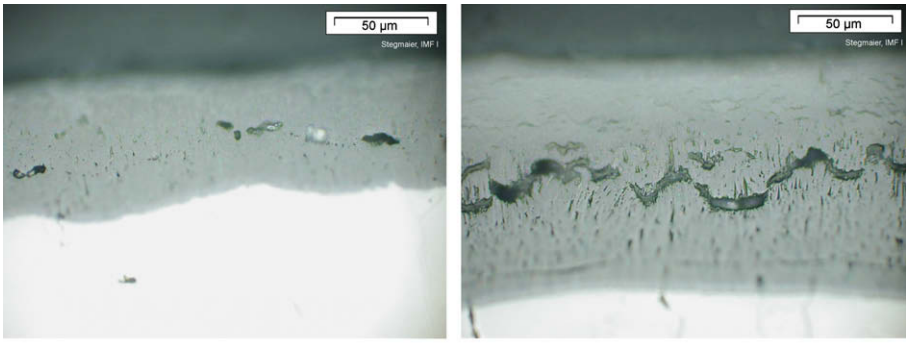

Fig. 10. Comparison of the optical micrographs of the crack structures in the oxide layer of the rods C and D after bundle test QUENCH-13.

4. Summary and conclusions

After steam oxidation the hydrogen concentration in the remaining metal of zirconium alloy claddings depends not only on temperature but as the discussion has shown it also seems to depend on the very local hydrogen partial pressure at the oxide/metal interface. The hydrogen partial pressure depends on the oxidation rate which is determined by temperature and crystallographic structure of the formed oxide layer. Additionally, the hydrogen partial pressure is strongly influenced by the oxide morphology. Cracks in the oxide layer results in hydrogen enrichment close to the metal surface. Open cracks can act as a 'hydrogen pump'.

The results show that the hydrogen uptake of zirconium alloys during steam oxidation cannot be estimated from temperature and time data alone. The processes connected with the monoclinic – tetragonal phase transition in the oxide have to be taken into account for prediction of hydrogen absorption and release during LOCA and severe accident scenarios.

Acknowledgment

This work is based on experiments performed at the ICON facility of the Swiss spallation neutron source SINQ, PSI, Villigen, Switzerland. The authors thank G. Frei, from PSI-ASQ for his support during the radiography experiments and U. Stegmaier and P. Severloh from FZK-IMF1 for the metallographic investigations.

References

[1] L. Sepold, P. Hofmann, W. Leiling, A. Miassoedov, D. Piel, L. Schmidt, M. Steinbrück, Nucl. Eng. Design 204 (2001) 205.
[2] M. Steinbrück, Status of the QUENCH Program, in: Proceedings of the 13th International QUENCH Workshop, November 20–22, Forschungszentrum Karlsruhe, ISBN 978-3-923704-63-7, 2007.
[3] L.K. Sepold, A. Miassoedov, G. Schanz, U. Stegmaier, M. Steinbrueck, J. Stuckert, Nucl. Technol. 147 (2004) 202.
[4] C. Degueldre, A. Amato, G. Bart, Scripta Materialia 54 (2006) 1211.
[5] J. Böhmert, M. Dietrich, J. Linek, Nucl. Eng. Design 147 (1993) 53.
[6] J. Freska, G. Konczos, L. Maroti, L. Matus, Oxidation and hydration of Zr 1% Nb alloys by steam, KFKI-Report-1995-17/G, 1995.
[7] J.H. Baek, Y.H. Jeong, J. Nucl. Mater. 372 (2008) 152.
[8] Z. Hozer, C. Györi, L. Matus, M. Horvath, J. Nucl. Mater. 373 (2008) 415.
[9] M. Grosse, M. Steinbrueck, E. Lehmann, P. Vontobel, Oxid. Met. 70 (2008) 149.
[10] M.S. Veshchunov, A.V. Berdyshev, J. Nucl. Mater. 255 (1998) 250.
[11] M. Steinbrück, J. Nucl. Mater. 334 (2004) 58.
[12] M. Grosse, G. Kuehne, M. Steinbrueck, E. Lehmann, J. Stuckert, J. Phys.: Condens. Matt. 20 (2008) 104263.
[13] M. Grosse, Comparison of the high temperature steam oxidation kinetics of advanced cladding materials, in: Proceedings 2008 International Congress on Advances in Nuclear Power Plants (ICAPP '08) Anaheim, June 8–12, California, USA, 2008.
[14] J. Stuckert, L. Sepold, M. Steinbrueck, Results of the QUENCH-12 reflood experiment with a VVER-type bundle, in: Proceedings of 15th International Conference on Nuclear Engineering (ICONE-15) Nagoya/Japan, CD-ROM Paper ICONE-15-10257, 2007.
[15] J. Stuckert, First results of the QUENCH-13 bundle experiment with silver–indium–cadmium control rod, in: Proceedings of the 13th International QUENCH Workshop, November 20–22, Forschungszentrum Karlsruhe, ISBN 978-3-923704-63-7, 2007.
[16] M. Grosse, E. Lehmann, P. Vontobel, M. Steinbrueck, Nucl. Instrum. Meth. A 566 (2006) 739.
[17] G. Kühne, G. Frei, E. Lehmann, P. Vontobel, Nucl. Instrum. Meth. A 542 (2005) 264.
[18] G. Schanz, Semi-mechanistic approach for the kinetic evaluation of experiments on the oxidation of zirconium alloys, Forschungszentrum Karlsruhe, Report FZKA-7329, 2007.